

# Study of a high power sine waveguide traveling wave tube amplifier centered at 8 GHz

Brad W. Hoff, David S. Simon, David M. French, Y. Y. Lau, and Patrick Wong

Citation: *Physics of Plasmas* **23**, 103102 (2016); doi: 10.1063/1.4964141

View online: <http://dx.doi.org/10.1063/1.4964141>

View Table of Contents: <http://aip.scitation.org/toc/php/23/10>

Published by the [American Institute of Physics](#)

---

## Articles you may be interested in

[Novel low-voltage subterahertz-range radial backward wave oscillator](#)  
*Physics of Plasmas* **24**, 013109 (2017); 10.1063/1.4973657

[A watt-class 1-THz backward-wave oscillator based on sine waveguide](#)  
*Physics of Plasmas* **19**, 013113 (2012); 10.1063/1.3677889

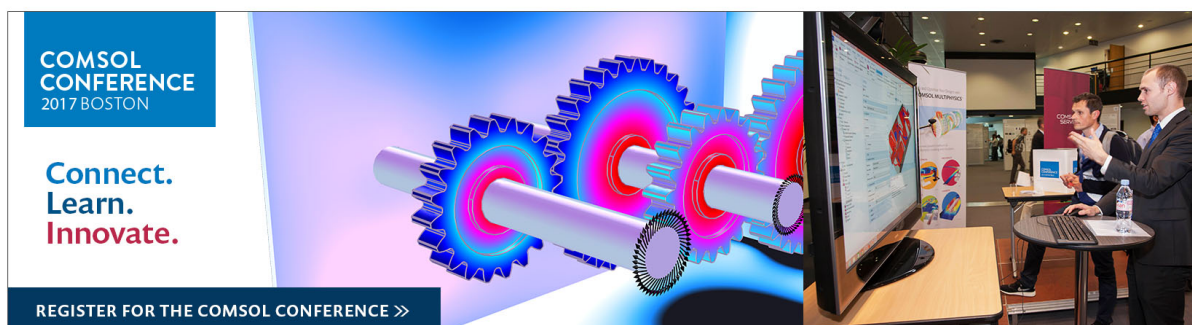
[Investigation of 0.38 THz backward-wave oscillator based on slotted sine waveguide and pencil electron beam](#)  
*Physics of Plasmas* **23**, 033111 (2016); 10.1063/1.4943410

[Chaotic millimeter wave generation in a helical-waveguide gyro-TWT with delayed feedback](#)  
*Physics of Plasmas* **23**, 103106 (2016); 10.1063/1.4964918

[Linear analysis of a W band groove-loaded folded waveguide traveling wave tube](#)  
*Physics of Plasmas* **17**, 113305 (2010); 10.1063/1.3511773

[Nonlinear shearing modes approach to the diocotron instability of a planar electron strip](#)  
*Physics of Plasmas* **22**, 092125 (2015); 10.1063/1.4931078

---



COMSOL CONFERENCE  
2017 BOSTON

Connect.  
Learn.  
Innovate.

REGISTER FOR THE COMSOL CONFERENCE >>

The image shows a promotional banner for the COMSOL Conference 2017 in Boston. The banner features a blue and white color scheme with the text 'COMSOL CONFERENCE 2017 BOSTON' and the slogan 'Connect. Learn. Innovate.' Below the text is a graphic of three interlocking gears with a glowing blue and red light effect. To the right of the banner is a photograph of a booth at the conference, showing a man in a suit standing next to a computer monitor displaying a presentation, with another person visible in the background.

# Study of a high power sine waveguide traveling wave tube amplifier centered at 8 GHz

Brad W. Hoff,<sup>1</sup> David S. Simon,<sup>2</sup> David M. French,<sup>2</sup> Y. Y. Lau,<sup>3</sup> and Patrick Wong<sup>3</sup>

<sup>1</sup>Air Force Research Laboratory, Kirtland AFB, Albuquerque, New Mexico 87117, USA

<sup>2</sup>Leidos, 2109 Airpark Road SE, Albuquerque, New Mexico 87106, USA

<sup>3</sup>Nuclear Engineering and Radiological Sciences Department, University of Michigan, Ann Arbor, Michigan 48109, USA

(Received 16 July 2016; accepted 18 September 2016; published online 6 October 2016)

Performance of a 20-stage X-band sine waveguide amplifier, driven by a 40 A, 100 kV, cylindrical electron beam, is studied using numerical simulation and interpreted using Pierce's classical traveling wave tube theory. For an input signal power level of 1.8 kW, particle-in-cell simulations predict gain and bandwidth values exceeding 14 dB and 13%, respectively. For an input signal power level of 7.2 kW, particle-in-cell simulations predict gain and bandwidth values exceeding 12 dB and 15%, respectively, with output power levels exceeding 110 kW at peak gain. Also given are: an assessment of the space charge factor (Pierce's QC parameter) for the complex circuit using simulation data, and an evaluation of the harmonic contents in the beam current.

[<http://dx.doi.org/10.1063/1.4964141>]

## I. INTRODUCTION

High power traveling wave tube (TWT) amplifiers are an integral part of RF systems used for applications such as radars and electromagnetic effects testing. In examining various traveling wave tube configurations, coupled cavity TWTs typically have the highest power outputs (ranging from 10s of kW to a few MW, pulsed). Reported gain values for coupled cavity TWTs have been as high as 35 dB with bandwidths ranging from 2% to 18%.<sup>1</sup> Because of the relative complexity associated with the fabrication of coupled cavity TWTs, the authors chose to explore other, geometrically simpler TWT configurations to determine high power scaling. The TWT configuration chosen for the present study and future experiment is a sine waveguide TWT.<sup>2</sup> The slow wave structure of the sine waveguide TWT consists of a rectangular waveguide that is sinusoidally displaced along the propagation axis in a direction perpendicular to the H-plane. This sine waveguide slow wave structure, evolved from a staggered double-grating waveguide amplifier concept,<sup>3</sup> has previously been explored as a potential THz "sheet beam" amplifier,<sup>1</sup> as a THz backward wave oscillator (BWO) utilizing a "sheet beam,"<sup>4</sup> and as a 380 GHz BWO utilizing a "pencil beam."<sup>5</sup> In the present study, the authors use both numerical simulation and analytic Pierce theory to investigate the viability of this structure as a high power X-band TWT amplifier, driven by a single electron "pencil beam." The new feature of this paper, which is rarely addressed in most publications on TWT designs because of its complexities, is our attempt to assess Pierce's space charge factor, QC, from simulations. The values of QC determined for the amplifier are compared to those calculated using methods prescribed by the literature. We also evaluate, numerically, the harmonic contents that result from the kinematic bunching (i.e., from the orbital crowding, as in a klystron) in the electron beam.

## II. SIMULATION GEOMETRY AND SETUP

Particle-in-cell simulations used to investigate the performance of a "pencil beam" driven sine waveguide TWT were accomplished using ICEPIC.<sup>6</sup> All ICEPIC simulations were performed using 0.5 mm × 0.5 mm × 0.5 mm grid resolution. Figures 1(a) and 1(b) provide 2-D and 3-D geometric views of the sine waveguide TWT simulated in the present study. At either end of the waveguide, within the upswept sections, perfectly matched layer (PML)<sup>7</sup> was used as an RF termination. An RF TE<sub>01</sub> mode launching surface was positioned just below the PML boundary at Y = 6 cm. The waveguide initially started out with a WR-90 cross section (1.02 cm × 2.29 cm), but following the curved section containing the beam pipe penetration, the waveguide height transitions from 1.02 cm to 1.90 cm before the start of the slow wave structure.

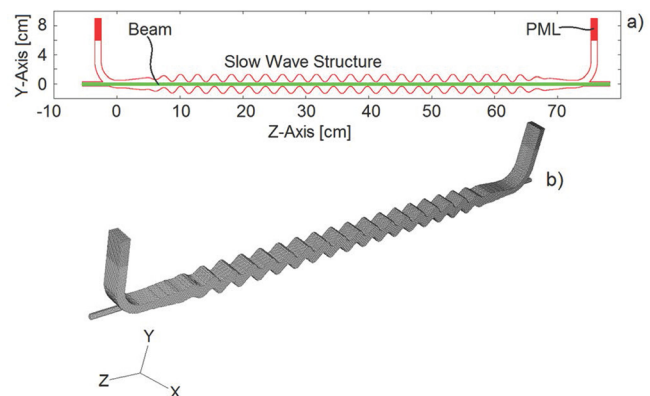


FIG. 1. (a) 2-D cross section geometry of the simulated sine waveguide TWT. (b) 3-D mesh plot example of a simulated sine waveguide TWT geometry (the displayed TWT mesh plot is 5 periods shorter than the simulated device used in this study, giving a better aspect ratio in the figure). Waveguide width in the X-Axis direction is 2.29 cm.

The simulated slow wave structure consisted of 20 periods, each of which was 2.7 cm long. These 20 periods have a displacement amplitude of 5 mm. In Figure 1, the full-height region of the slow wave structure (SWS) begins at  $Z = 9.4$  cm and ends at  $Z = 63.4$  cm. On both the input and output sides of the full-height SWS section were sets of two taper periods in which the displacement amplitude was linearly tapered to zero. The walls of the structure were assigned a conductivity of  $1.334 \times 10^6$  S/m, consistent with stainless steel.

The radius of the beam pipe, in which the beam is launched, was 4.5 mm and the beam radius is 2.5 mm. A separation of at least 2.0 mm is maintained between the beam outer radius and the rippled upper and lower walls of the waveguide. The slow wave structure was immersed in a 0.3 T axial magnetic field, aligned along the Z direction. Simulation hot tests utilized a zero temperature electron beam with a voltage of 100 kV with a current of 40 A. The 0.3 T axial magnetic field was found to be sufficient to prevent intersection of the 40 A beam with the walls of the device in all hot test simulations performed in this study.

Previously published sine waveguide TWT amplifier configurations<sup>2</sup> as well as TWTs based on the structurally similar staggered-grid slow wave structure,<sup>8</sup> utilize a sheet-like electron beam to drive the amplifier. Sheet-like electron beams are highly susceptible to the diocotron instability, which results in distortion and curling of the edges of the sheet beam.<sup>8–11</sup> Because the spatial growth rate of the diocotron instability tends to be very high, sheet beam TWTs must be very short, thus making them suited to small, high frequency, lower power amplifiers. Use of a cylindrical “pencil beam” avoids this instability, but does incur a penalty of reduced gain per period as compared with a sheet beam device.

### III. SIMULATION COLD TEST RESULTS

The dispersive properties of the slow wave structure were determined using the frequency domain code, ANSYS HFSS.<sup>12</sup> Master-slave bounded eigenmode solution data was calculated. The calculated dispersion data indicate pairs of modes, offset from each other by a  $2\pi$  phase shift, forming both the first and second pass bands, depicted in Figure 2. Distance along the  $kd$  axis represents the phase shift across a single SWS period. Also plotted in Figure 2 are the light line and the beam line for 100 kV. RF data from hot test simulations, discussed later in Section IV, did not yield noticeable microwave generating or amplifying interactions between the beam and modes 1b and 2b from Figure 2.

### IV. SIMULATION HOT TEST RESULTS AND DISCUSSION

As discussed previously in Section II, beam parameters for all hot test simulations were 100 kV and 40 A. The beam was ramped from 0 A to 40 A over a 10 ns time period. Prior to beginning gain studies with injected RF power, the TWT was verified to be zero drive (no input signal) stable for at least a full microsecond with these beam parameters. The distributed loss imposed by the previously described wall

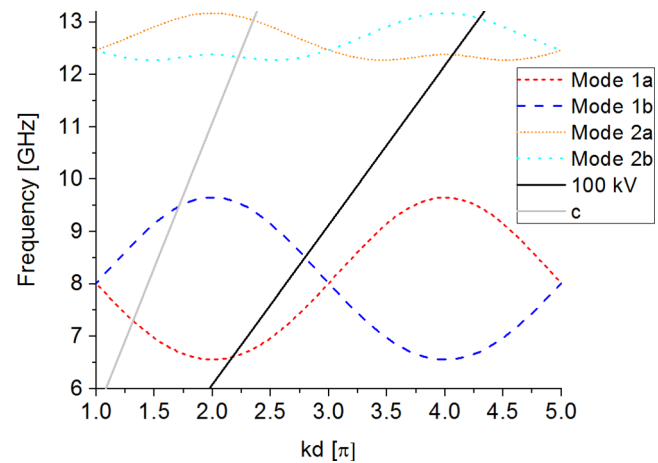


FIG. 2. Dispersion plot for the sine waveguide slow wave structure, where  $kd$  is the phase shift per SWS period. Also depicted are the light line and the 100 kV beam line.

conductivity within the TWT provided an adequate suppression of self-oscillation, in particular, near the band edge<sup>13</sup> of mode 2a, shown in Figure 2.

To study the gain of the TWT, input signals with frequencies between 7.0 and 9.0 GHz were injected in the upstream waveguide port of the amplifier. Three signal power levels (1.8 kW, 3.6 kW, and 7.2 kW) were utilized to excite the slow wave structure. In all simulations, after the injected beam current reached 40 A, the input RF signal was ramped from zero to the final power level over a period of 10 ns. The input RF power level was held constant for 110 ns and then ramped to 0. TWT gain for each of the input signal power level, plotted as a function of frequency is displayed in Figure 3. Bandwidth, defined as  $\Delta f/f_0$  (where  $\Delta f$  is the frequency range over which the gain exceeds  $-3$  dB from the peak gain and  $f_0$  is the center frequency of the aforementioned frequency range) was nominally around 13% but increased to 15% as the tube begins to approach saturation at an input power level of 7.2 kW.

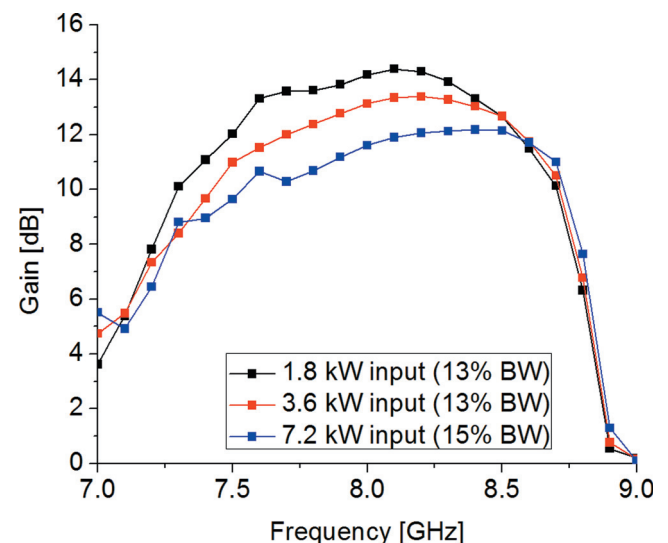


FIG. 3. Sine waveguide TWT gain as a function of frequency for input power levels of 1.8 kW, 3.6 kW, and 7.2 kW.

Output power of the amplifier for simulation cases using 1.8 kW, 3.6 kW, and 7.2 kW input signals at 8 GHz are plotted in Figure 4. The first portion of the power trace ( $\sim 10$  ns– $\sim 25$  ns) indicates the presence of impedance mismatches at the ends of the amplifier. Increasing the number of taper stages at either end of the full-height SWS was not found to substantially reduce the effect, indicating the probable source of the impedance mismatch is the beam pipe penetrations into the waveguide.

A phase space plot of particle axial velocity as a function of axial position is provided in Figure 5. Particle phase space data was sampled at  $t = 80$  ns for each of three 8 GHz cases previously discussed. The Z-axis of Figure 5 corresponds to that of Figure 1(a). The downstream end of the full-height SWS is located at  $Z = 63.4$  cm. The development of the so-called “Cutler spur” on the phase space plot, in which the velocity becomes multi-valued at a given position, indicates the onset of nonlinear operation as the amplifier progresses toward saturation with increased input power.<sup>14,15</sup> This effect is evident in the 7.2 kW input power case beginning in the vicinity of  $Z = 52$  cm. Plots of linear charge density as a function of axial position are displayed in Figure 6. In Figure 6 plot of the 7.2 kW input power case, the electron bunch density reaches a peak around  $Z = 52$  cm and then begins to decrease before the downstream end of the SWS ( $Z = 63.4$  cm). In all cases, some amount of de-bunching occurs beyond the end of the full-height section of the SWS as the RF wave loses synchronism with the electron beam. Electric field magnitude and Z-axis component plots of the 7.2 kW input power level case are provided in Figures 7(a) and 7(b), respectively.

In the 1.8 kW and 7.2 kW simulation cases, beam current was sampled at the end of the full-height section of the SWS ( $Z = 63.4$  cm). FFT magnitude plots of the ratio of sampled current at the end of the full-height SWS to input current as a function of frequency are provided in Figure 8. As described by Dong *et al.*,<sup>16</sup> and evident in Figure 8, a variety of harmonic AC can be generated on the beam, even

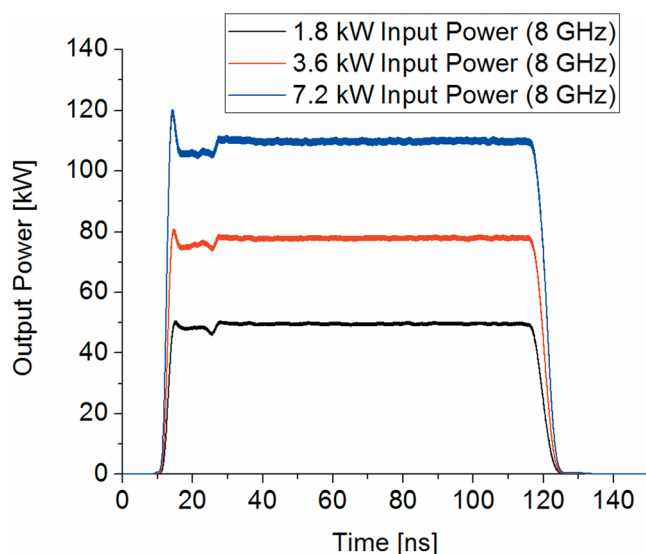


FIG. 4. Amplifier output power for 8 GHz input signals with power levels of 1.8 kW, 3.6 kW, and 7.2 kW.

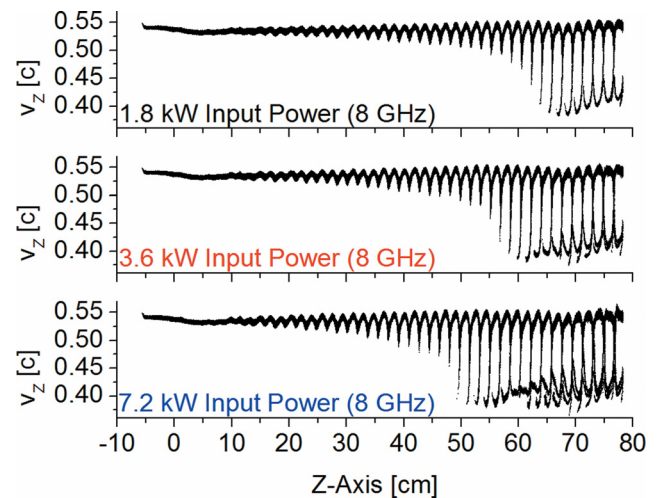


FIG. 5. Phase space plot at 80 ns for simulation cases using input power levels of 1.8 kW, 3.6 kW, and 7.2 kW.

when using only a single input frequency. The harmonic current is a significant fraction of the AC at the input (fundamental) frequency. While these harmonics could be problematic for amplifiers having multi-octave gain bandwidths, in configurations in which these harmonics do not fall within the amplification band, there is no intrinsic gain mechanism and the harmonic components are not strongly represented in the RF output of the device, as demonstrated in Figure 9. It should be noted that while the present amplifier configuration would be expected to be relatively insensitive to destabilization due to self-generated out-of-band harmonics, it would still be expected to be susceptible to destabilization by self-generated in-band harmonics and by sources of in-band reflections, such as those resulting from impedance mismatches due to fabrication imperfections, window junctions, and severs, etc.

## V. PIERCE ANALYSIS

The amplifier gain results discussed in Section IV are interpreted in terms of Pierce’s classical theory of

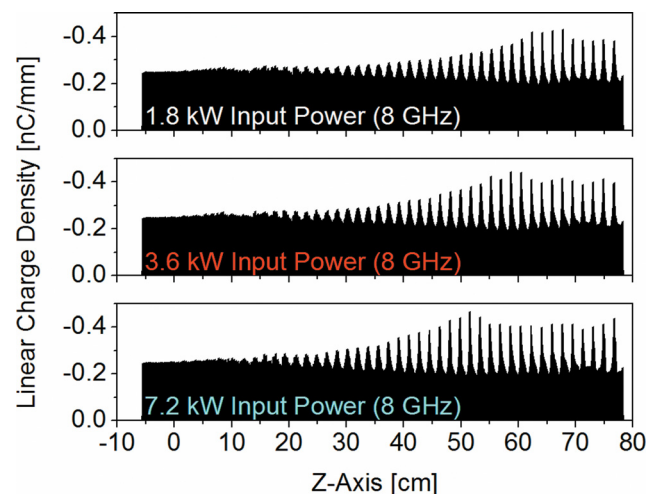


FIG. 6. Linear charge density as a function of axial position for the simulation cases previously described in Figure 5.



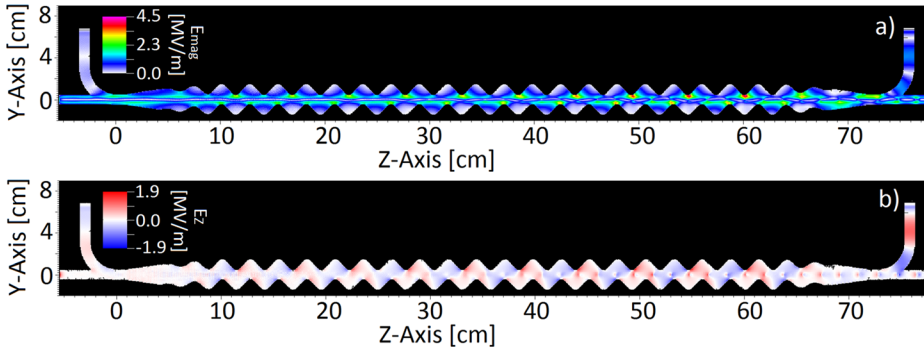


FIG. 7. Electric field magnitude pseudocolor plot (a) and axial electric field component pseudocolor plot (b) of the sine waveguide amplifier operating in steady state with an 8 GHz, 7.2 kW input signal.

TWTs.<sup>15–17</sup> Once the beam current, beam voltage, and the sine-waveguide geometry (including the cold-tube loss) are specified, the dimensionless gain parameter  $C$ , detune parameter  $b$ , and loss parameter  $d$ , in Pierce's theory<sup>15,17</sup> may be determined with the aid of the HFSS and ICEPIC codes. HFSS yields the interaction impedance,  $K$ , and the circuit wave's phase velocity,  $v_p$ , while the cold tube loss rate is extracted from ICEPIC, all of which may be used to determine  $C$ ,  $b$ , and  $d$ . The remaining parameter, Pierce's space charge parameter  $QC$ , cannot be easily calculated analytically for our geometry, which consists of a pencil beam in a planar sine waveguide. To gain a deeper understanding of the ICEPIC simulation results, and a better feel for the scaling of Pierce's space charge parameter for the sine waveguide TWT, we numerically solved for the value of  $QC$  that forced Pierce's TWT theory, given by Eq. (3) below, to match the gain values derived from the ICEPIC simulations for the 1.8 kW input power level cases depicted in Figure 3.

First, for a small signal electric field with  $e^{j\omega t - j\beta z}$  dependence, the complex propagation constant,  $\beta(\omega)$ , is determined from Pierce's 3-wave TWT dispersion relation<sup>15,17</sup>

$$(\delta^2 + 4QC)(\delta + jb + d) = -j, \quad (1)$$

where  $\delta = -j(\beta - \beta_e)/C\beta_e$ ,  $\beta_e = \omega/v_0$ ,  $b = (v_0/v_p - 1)/C$ ,  $v_0$  is the beam's DC velocity,  $v_p$  is the phase velocity of the slow wave structure in the absence of the beam, and  $d$  is the normalized cold tube circuit loss rate. For a relativistic beam, Pierce gain parameter,  $C$ , is given by<sup>18</sup>

$$C^3 = \frac{I_b K_0}{4V_b} \frac{2}{\gamma(\gamma + 1)}, \quad (2)$$

where  $K$  is the interaction impedance which may be inferred from HFSS, and  $\gamma = 1/\sqrt{1 - v_0^2/c^2}$  is the relativistic mass factor associated with the electron beam ( $\gamma = 1.1957$  for a 100 kV beam).

According to Pierce's TWT theory, the small signal gain (in power) in the circuit wave at a distance  $z$  downstream of the input wave at  $z=0$ , which is written as  $E_1(0, t) = E_{10}e^{j\omega_0 t}$ , is given by<sup>16</sup>

$$\left| \frac{E_1(z, t)}{E_1(0, t)} \right|^2 = \left| \sum_{i=1}^3 \alpha_i \delta_i^2 e^{C\delta_i (\frac{\omega_0 z}{v_0})} + 4QC \sum_{i=1}^3 \alpha_i e^{C\delta_i (\frac{\omega_0 z}{v_0})} \right|^2, \quad (3)$$

where  $\delta_i$ , ( $i = 1, 2$ , and  $3$ ) are the three complex roots to Eq. (1) at the input frequency  $\omega_0$ , and  $\alpha_i$ , ( $i = 1, 2$ , and  $3$ ), are the amplitudes of the three (3) modes on the TWT, obtained from the solution to

$$\begin{aligned} \alpha_1 + \alpha_2 + \alpha_3 &= 0, \\ \alpha_1 \delta_1 + \alpha_2 \delta_2 + \alpha_3 \delta_3 &= 0, \\ \alpha_1 \delta_1^2 + \alpha_2 \delta_2^2 + \alpha_3 \delta_3^2 &= 1. \end{aligned} \quad (4)$$

Note that the small signal gain given in Eq. (3) includes the launching loss because it accounts for all three modes of the Pierce dispersion relation, Eq. (1). Equation (3) has been

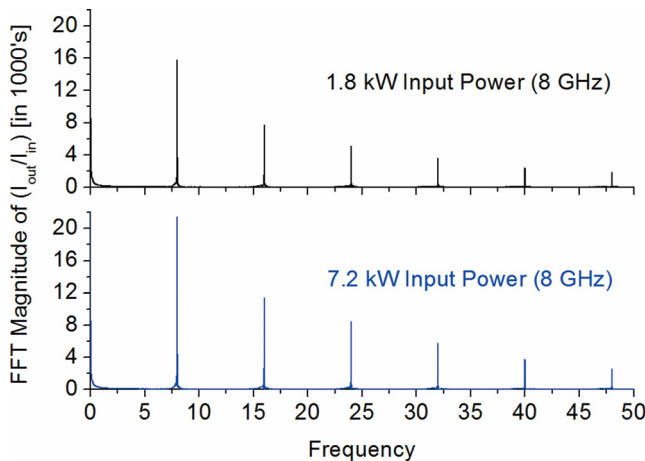


FIG. 8. FFT plots of the ratio of input to output current sampled at the beginning and end (respectively) of the SWS.

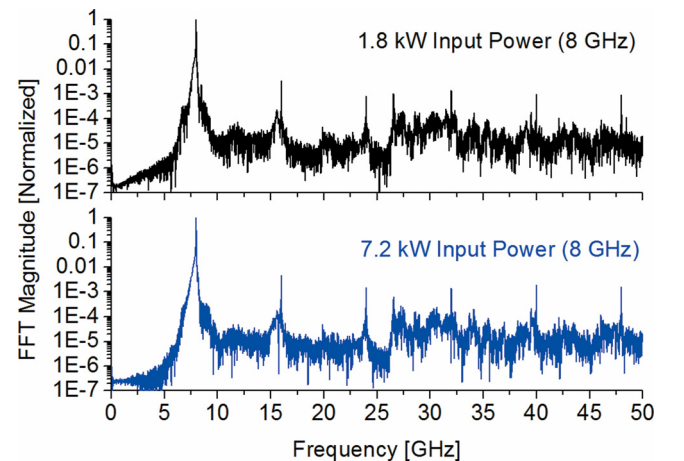


FIG. 9. FFT plots of the RF electric field measured across the extraction waveguide of the 1.8 kW and 7.2 kW input signal cases.

shown to be applicable even in the slightly nonlinear regime in several examples.<sup>16</sup>

Figure 3 shows the gain of the amplifier, obtained from ICEPIC for a 40 A, 100 kV beam subjected to a 1.8 kW drive over 7–9 GHz. Figure 10 shows the values of C, b, and d over this range of frequency obtained from HFSS. Also included in Figure 10 is the required value of QC so that the small signal theory, Eq. (3), matches the observed amplifier gain from the ICEPIC simulations for the 1.8 kW input power level cases, as shown in Figure 3. We should remark that the numerical value of Eq. (3) is sensitive to the value of QC, which, as mentioned previously, is difficult to determine analytically.<sup>19</sup>

The commonly used method of approximating the space charge term, QC, relies on finding the plasma reduction factor, R, under the assumption that the drift tube is smooth. The reduction factors for a very wide range of common geometries were analyzed and tabulated by Branch and Mirhan,<sup>20</sup> along with a relation between QC and the plasma frequency reduction factor, R<sup>21</sup>

$$\sqrt{4QC^3} = \frac{R\omega_p/\omega}{1 + R\omega_p/\omega}. \quad (5)$$

The sine waveguide consists of a pencil beam in a rectangular waveguide (which is complex, and not covered in the literature), so the reduction factor R, which is independent of the beam current,<sup>20</sup> will be approximated in two ways, as a pencil beam in a cylindrical waveguide, and as a sheet beam between parallel plates. For both approximations, the size of the smooth waveguide is taken to be the average of the sine waveguide, i.e., 1.9 cm separation for the parallel plates and 1.9 cm diameter for the cylinder.

The resulting values of QC, with C being given in Fig. 10 and Q obtained from Eq. (5), are plotted in Figure 11. Figure 11 shows a poor match to the QC values found from the simulation. The resulting gain is very sensitive to QC, so the

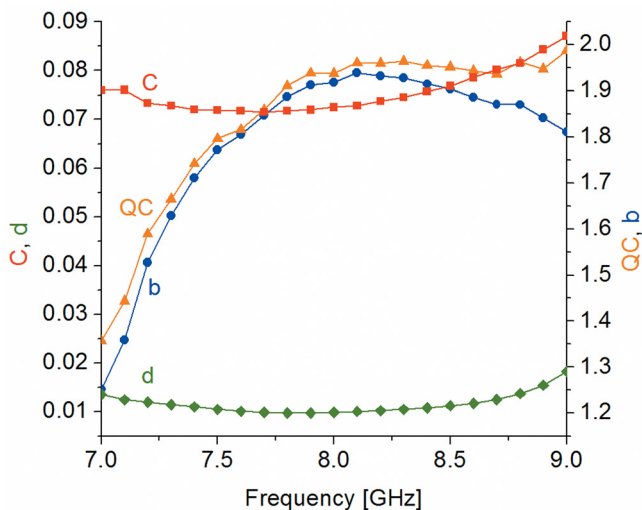


FIG. 10. Values of C, b, and d for a sine-waveguide TWT driven by a 40 A, 100 kV pencil beam. The interaction impedance and circuit phase velocity used in C and b were obtained from HFSS. Also shown are the values of QC required to match the 1.8 kW input power level cases of Figure 3 with Pierce's 3-wave TWT theory, Eq. (3).

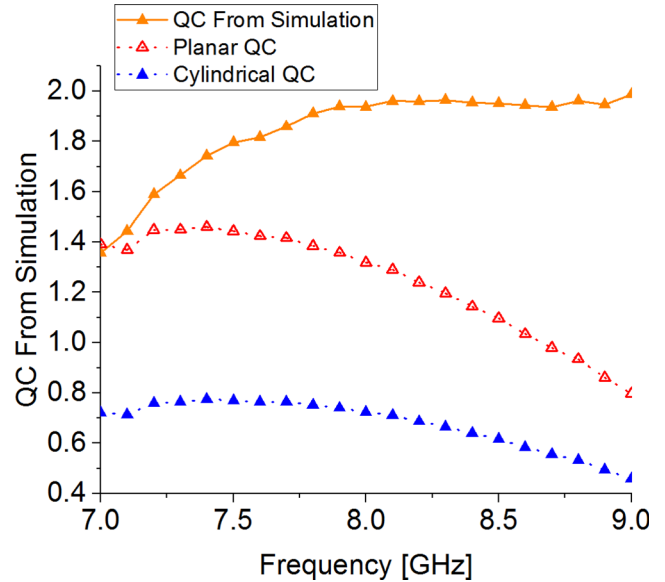


FIG. 11. A comparison of QC values calculated using inputs from simulation hot tests and QC values estimated using methods provided in the published literature.<sup>20,21</sup>

approximated QC values result in vastly larger gains than simulation. At 8 GHz, the simulation gain is 14.2 dB. Pierce analysis using the planar QC would result in a gain of 37.3 dB, and using the cylindrical QC would produce 45.2 dB.

## VI. CONCLUSIONS

The performance of a high power X-band sine waveguide TWT amplifier was studied using numerical simulation and interpreted in terms of Pierce's classical theory of TWTs. The 20-stage amplifier model incorporated realistic wall loss (for a tube comprised of stainless steel) and was driven by a cylindrical electron beam with a current of 40 A and a voltage of 100 kV. For an input signal power level of 1.8 kW, ICEPIC simulations predict gain and bandwidth values exceeding 14 dB and 13%, respectively. For an input signal power level of 7.2 kW, ICEPIC simulations predict gain and bandwidth values exceeding 12 dB and 15%. Output power levels exceeding 110 kW at peak gain are achievable, in simulation, when using an input signal power level of 7.2 kW. TWT simulation results were used to determine values for Pierce's space charge factor, QC. Comparisons of QC values determined using simulation hot test data were found to differ substantially from values estimated using existing published methods.

## ACKNOWLEDGMENTS

This work was supported in part by the Air Force Office of Scientific Research under Grant Nos. AFOSR LRIR 16RDCOR310 and FA9550-15-1-0097, in part by the Air Force Research Laboratory, and in part by the Department of Defense High Performance Computing Modernization Program under Grant No. AFDEK01314625. The authors wish to acknowledge D. P. Chernin of Leidos for his helpful discussions.

- <sup>1</sup>R. J. Barker and E. Schamiloglu, *High-Power Microwave Source and Technologies* (Wiley-IEEE Press, New York, 2001).
- <sup>2</sup>X. Xu, Y. Wei, F. Shen, Z. Duan, Y. Gong, H. Yin, and W. Wang, *IEEE Electron Device Lett.* **32**(8), 1152 (2011).
- <sup>3</sup>Y. Shin, L. R. Barnett, and N. C. Luhmann, Jr., *Appl. Phys. Lett.* **93**(22), 221504-1–221504-3 (2008).
- <sup>4</sup>X. Xu, Y. Wei, F. Shen, H. Yin, J. Xu, Y. Gong, and W. Wang, *Phys. Plasmas* **19**, 013113 (2012).
- <sup>5</sup>L. Zhang, Y. Wei, B. Wang, W. Shen, J. Xu, Y. Gong, and G. Park, *Phys. Plasmas* **23**, 033111 (2016).
- <sup>6</sup>R. E. Peterkin and J. W. Luginsland, *Comput. Sci. Eng.* **4**(2), 42–49 (2002).
- <sup>7</sup>J. Berenger, *J. Comput. Phys.* **114**, 185–200 (1994).
- <sup>8</sup>P. C. Panda, V. Srivastava, and A. Vohra, *IEEE Trans. Plasma Sci.* **41**(3), 461 (2013).
- <sup>9</sup>C. Ruan, S. Wang, Y. Han, Q. Li, and X. Yang, *IEEE Trans. Electron Devices* **61**(6), 1643 (2014).
- <sup>10</sup>H. S. Uhm, S. Ben-Manahem, and D. Yu, *Phys. Plasmas* **1**, 3686 (1994).
- <sup>11</sup>J. H. Booske, *Phys. Plasmas* **15**, 055502 (2008).
- <sup>12</sup>See <http://www.ansys.com/Products/Electronics/ANSYS-HFSS> for ANSYS HFSS.
- <sup>13</sup>D. M. H. Hung, I. M. Rittersdorf, P. Zhang, D. Chernin, Y. Y. Lau, T. M. Antonsen, Jr., J. W. Luginsland, D. H. Simon, and R. M. Gilgenbach, *Phys. Rev. Lett.* **115**, 124801 (2015).
- <sup>14</sup>C. C. Cutler, *Bell Syst. Tech. J.* **35**, 841–876 (1956).
- <sup>15</sup>A. S. Gilmour, Jr., *Principles of Traveling Wave Tubes* (Artech House, Norwood, 1994).
- <sup>16</sup>C. F. Dong, P. Zhang, D. Chernin, Y. Y. Lau, B. W. Hoff, D. H. Simon, P. Wong, G. B. Greening, and R. M. Gilgenbach, *IEEE Trans. Electron Devices* **62**(12), 4285–4292 (2015).
- <sup>17</sup>J. R. Pierce, *Traveling Wave Tubes* (Van Nostrand, New York, 1950).
- <sup>18</sup>T. Kimura, S. Alberti, B. G. Danly, and R. J. Temkin, “Long-pulse, high-power, x-band relativistic traveling-wave tube amplifier,” in *Proceedings of the International Conference on Particle Accelerator* (IEEE, Washington, DC, 1993), Vol. 4, pp. 2690–2692.
- <sup>19</sup>Y. Y. Lau and D. Chernin, *Phys. Fluids B* **4**, 3473 (1992).
- <sup>20</sup>G. M. Branch and T. G. Mihran, “Plasma frequency reduction factors in electron beams,” *IRE Transactions on Electron Device* **2**(2), 3–11 (1955).
- <sup>21</sup>C. K. Birdsall and G. R. Brewer, “Traveling-wave tube characteristics for finite values of C,” *Transactions of the IRE Professional Group on Electron Devices ED-1*(3), 1–11 (1954).